A Study on Dimensional Parameters of Shell-to-Bottom Weld Area in Molten Salt Storage Tanks

Yiming Xue*, Qipeng Song, Wei Zhao, Yingchun Wang, Dengyun Zhao, Kang Chen

Northwest Engineering Corporation Limited of POWERCHINA, Xian 710000, China

*xym13020@163.com

Abstract. The molten salt storage tank is a key component of the solar thermal power plant's energy storage system. In the structure of the tank, the region with shell-to-bottom weld is a weak area that affects the safe operation of the tank. This study focuses on the design of a storage tank in a solar thermal project in Qinghai Province, and uses the ABAQUS finite element thermal-stress coupling analysis method to investigate the influence of the first layer tank wall thickness, edge plate extension length, and edge plate thickness in the region of shell-to-bottom weld. The aim is to provide reference for the design of future molten salt storage tanks. The research results indicate that increasing the thickness of the tank wall and bottom plate are both beneficial for reducing the peak stress in the region of shell-to-bottom weld. The extension length of the edge plate has a significant impact on the stress in the bottom plate. When the extension length is too small or too large, it leads to uneven distribution of peak stress in the bottom plate. When the extension length exceeds 200mm, it no longer has a significant impact on the stress in the bottom plate, the peak stress in the region of shell-to-bottom weld, and the deformation of the bottom plate.

Keywords: Molten salt storage tank; Finite element analysis; Thermal coupling; Stress field; Shell-to-Bottom Weld; Parameter Study

1 Introduction

During the operation of a concentrated solar power plant, molten salt tanks play a crucial role[1, 2]. These tanks serve as the primary storage vessels for molten salt, tasked not only with enduring significant thermal stresses induced by high temperatures but also ensuring structural stability and safety under various operational conditions[3].

Previous research has focused on the stress analysis of molten salt tank structures. Zeng et al. [4] evaluated stress distribution at the weld seams of a 20m diameter tank using regulatory guidelines. Tang et al. [5] computed deformation and stress distribution of tank walls under steady-state conditions, conducting stress assessments. Zhang et al. [6] performed structural static analysis using ABAQUS finite element software, evaluating stress in the tanks. Gao [7] established a finite element model in ANSYS to analyze stress and temperature distribution under static conditions. Wan [8] evaluated temperature distribution using a coupled thermal performance model, studying mechanical

Z. Zhang et al. (eds.), *Proceedings of the 2024 6th International Conference on Structural Seismic and Civil Engineering Research (ICSSCER 2024)*, Advances in Engineering Research 246,
https://doi.org/10.2991/978-94-6463-556-0_7

performance via finite element modeling across various temperature conditions. Zhang et al. [9] simulated thermal stresses using sequential thermal-structural coupling, assessing stress per the third strength theory.

In operational concentrated solar power plants, molten salt tank leaks have occurred frequently. The integrity and stability of the shell-to-bottom weld, critical connections between tank walls and bottoms, directly impact the structural safety of the entire tank system.

However, in the current research mentioned earlier, there is relatively little research on the geometric dimensions related to the shell-to-bottom weld area, and there is a lack of reference in actual engineering design. This article uses ABAQUSY finite element software to conduct parameter sensitivity analysis on three important geometric dimensions of the shell-to-bottom weld area, including the thickness of the first layer of tank wall, the extension length of the edge plate, and the thickness of the edge plate. Intended to provide reference and basis for the design of molten salt storage tanks, filling the gap in the study of the size of the shell-to-bottom weld area.

2 Introduction to Finite Element Models

2.1 Basic Information of Molten Salt Storage Tanks

Structural Information of Molten Salt Storage Tanks

This article is based on a solar thermal project in Qinghai Province, and selects high-temperature molten salt storage tanks with higher temperatures as the research object. The structural design of the molten salt storage tank is carried out using the change point design method and relevant design basis in the API650 standard. The high-temperature molten salt storage tank body is mainly composed of a top mesh shell structure, a top plate, a tank wall plate, and a tank bottom plate. The arch has a height of 4.51m and a curvature radius of 40.2m. The tank wall panel is divided into 6 layers from bottom to top along the height direction, with each layer having a height of 2.5m. The thickness gradually decreases from bottom to top, showing a stepped change. The tank wall panel adopts a centerline aligned installation method. The radius of the molten salt storage tank is 18.72m. The bottom plate of the tank is divided into the first ring of annular edge plate, the second ring of annular edge plate, and the center plate from the outside to the inside, and the thickness decreases sequentially. The specific dimensions of the tank wall panel and tank bottom plate are shown in the Table 1. The geometric dimensions of the molten salt storage tank in this project are shown in Fig. 1.

Table 1. Dimensions of wall and bottom plates for high-temperature molten salt storage tanks

Part		Plate thickness (mm)	Plate width (mm)
Number of wall panel layers	First layer	54	2500
	Second layer	43	
	Third layer	33	
	Fourth layer	24	
	Fifth layer	15	

	Sixth layer	12	
Tank bottom plates	First annular edge plate	43	1250
	Second annular edge plate	24	1250
	Middle panel	12	\
Edge plate extension length		\	150

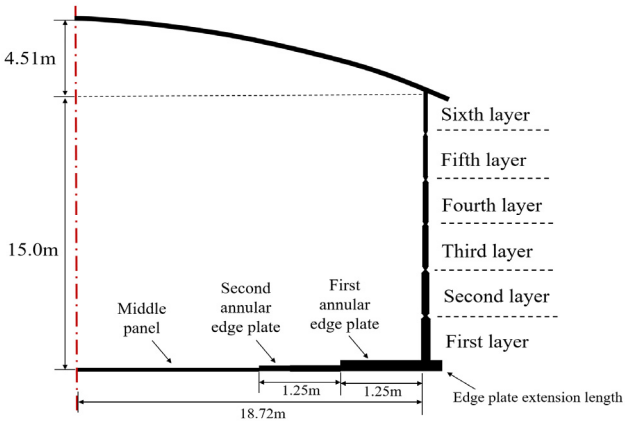

Fig. 1. Geometric dimension diagram of molten salt storage tank

Material Properties

At present, the steel used for high-temperature molten salt storage tanks is mainly 347H stainless steel. 347H stainless steel has excellent high-temperature strength and corrosion resistance, and can maintain stable structure and performance under high temperature conditions. In addition, during the modeling process, corrosion allowance is considered according to the API650 specification. The parameters of 347H in an environment of 575℃ are shown in **Table 2**.

Table 2. 347H parameters

Items	347H (575°C)
Allowable stress (MPa)	92.3
Yield stress (MPa)	130
Elastic modulus (GPa)	154
Poisson's ratio	0.3
Coefficient of thermal expansion (10^{-6}/°C)	18.71
Thermal conductivity coefficient (W/(m*°C))	21.3
Density (kg/m^3)	7980
Corrosion allowance (mm)	1.3

Load Situation

In the numerical simulation process, the main loads considered are self weight load, molten salt pressure, design internal pressure, live load, and temperature load, with specific values shown in **Table 3**. The friction coefficient between the bottom plate of the molten salt storage tank and the foundation surface in the calculation is 0.5

Table 3. Load Value Table

Items		Value
Dead load	Tank weight	Based on density 7980kg/m3
	Self weight of insulation layer	1.12kPa
	Self weight of tank top steel plate	0.5kPa
Molten salt pressure		Molten salt density 1725kg/m3 Maximum liquid level 13.65m Maximum pressure 235.5kPa
Design pressure of storage tank		-0.25kPa~0.5kPa
Live load		0.72kPa[10]

2.2 Establishment of the Finite Element Model

In this study, the main focus is on the stress distribution of the wall panels, bottom plates, and shell-to-bottom weld areas of molten salt storage tanks. Therefore, in the modeling process, the mesh shell structure of the tank top is simplified and only the model of the tank top steel plate is established. In addition, the molten salt storage tank has symmetry in structure and load, so the planar axisymmetric modeling method is chosen for modeling. This processing method can not only improve calculation efficiency but also ensure calculation accuracy. The schematic diagram of the finite element model grid established in this study is shown in **Fig. 2**.

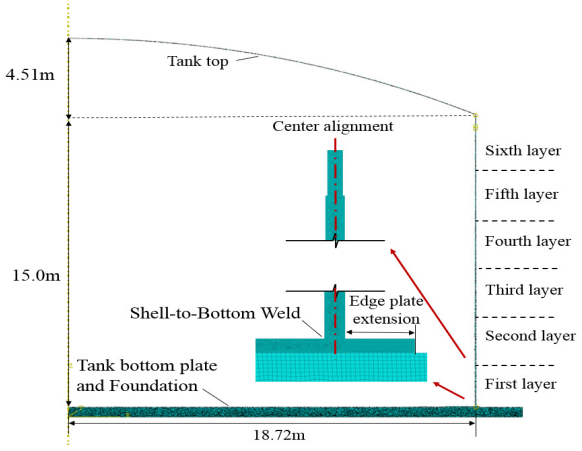

Fig. 2. Finite element model and mesh diagram

2.3 Finite Element Model Validation

Molten salt storage tanks belong to cylindrical thin-walled containers with free boundaries, uniform cross-sections and materials, and are not affected by concentrated loads. When receiving the hydrostatic pressure of molten salt in the storage tank, the radial deformation of the tank wall panel can be calculated using the thin plate theory, as shown in equation (1).

$$\Delta R = \frac{\sigma R}{E} \tag{1}$$

$$\sigma = \frac{pD}{2\delta} \tag{2}$$

where, ΔR is the radial deformation of the thin-walled container; σ is the circumferential stress of the wall panel; E is the elastic modulus of the material; σ is the pressure acting on the inner wall of the molten salt storage tank; D is the diameter of the storage tank; δ is the thickness of the tank wall.

As shown in **Fig. 3**, the radial deformation curves of the tank wall plate exhibit characteristic fluctuations and abrupt changes in both theoretical calculations and numerical simulations. The theoretical calculation results show a linear variation, while the numerical simulation curves are smoother due to stress equilibrium between elements. Discrepancies in axial deformation at lower wall heights occur because the numerical simulations account for friction between the tank bottom plate and the foundation, which is not considered in the theoretical calculations.

Overall, the numerical model results align well with the theoretical calculations, validating the accuracy and effectiveness of the finite element model established in this study.

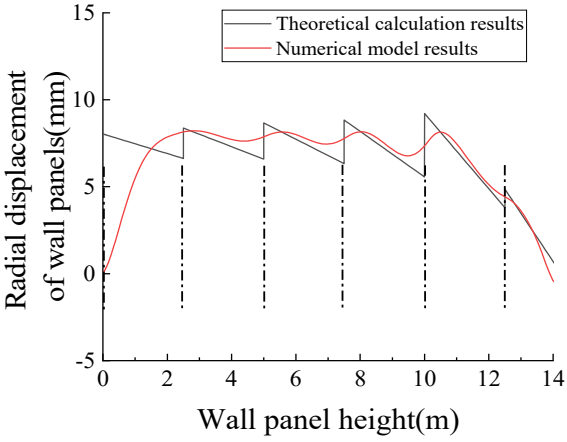

Fig. 3. Comparison between numerical models and theoretical calculation results

3 Study on the Influence of Wall Panel Size on Stress

Due to the similarity between the molten salt pressure acting on the walls of molten salt tanks and hydrostatic pressure, the maximum pressure occurs at the bottom and decreases gradually upwards. Under uniform internal pressure, the wall primarily experiences hoop stress, leading to a decreasing thickness from bottom to top.

However, the first layer of tank wall at the bottom interacts with the foundation through friction, which restricts tank deformation. Therefore, the first layer of wall not only experiences hoop stress but also axial and radial stresses, especially near the shell-to-bottom weld area, resulting in a complex stress state. Therefore, it is necessary to analyze and study the thickness of the first layer of wall panels

Based on the completed dimensions of the molten salt tank detailed in Section 2.1, this section aims to optimize the thickness of the wall panels and analyze the effect of wall panel thickness on stress. To achieve this, the stress distribution of the first layer wall was studied under various thicknesses: 48 mm, 50 mm, 52 mm, 54 mm, 56 mm, 58 mm, and 60 mm.

Fig. 4 illustrates the Mises stress on the inner and outer sides of the tank wall at different thicknesses of the first layer. The X-axis represents the height of the wall, where 0m to 2.5m corresponds to the first layer and 2.5m to 5m to the second layer. The figure shows that varying the thickness of the first layer significantly affects stress distribution in that layer but has minimal impact on the second layer. Generally, increasing the tank wall thickness results in an overall reduction of stress on both the inner and outer sides of the tank wall.

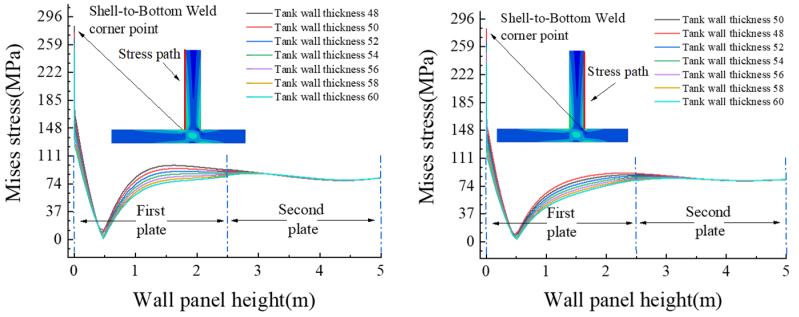

Fig. 4. Stress variation curves of the tank wall with different wall thicknesses: (a) Inner wall (b) Outer wall

Fig. 5 shows the relationship between Mises stress on the inner and outer sides of the tank wall at heights of 1.5m and 2.5m, plotted against tank wall thickness. The graph reveals that the tank wall stress decreases linearly with increasing wall thickness. At a height of 1.5m, the slope of the stress variation curve with wall thickness is greater than at 2.5m, indicating a larger impact of wall thickness on stress in the middle section of the tank wall.

On the inner side of the tank wall, when the thickness is less than 52mm, the stress at 1.5m is greater than at 2.5m. However, with increasing thickness, the stress at 2.5m gradually exceeds that at 1.5m. On the outer side of the tank wall, the stress at 2.5m is consistently greater than at 1.5m.

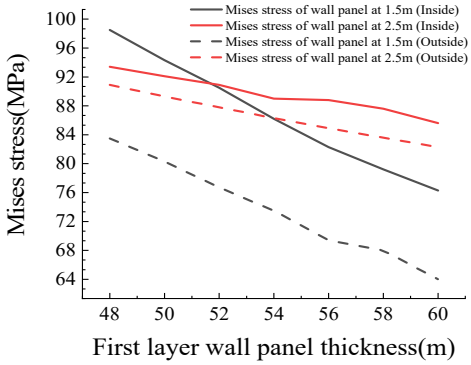

Fig. 5. Stress versus wall thickness curves at 1.5m and 2.5m positions of the tank wall

Fig. 6 displays the variation of maximum Mises stress on the inner and outer sides of the tank wall weld seam with respect to tank wall thickness. As the tank wall thickness increases, both the maximum stresses on the inner and outer sides of the weld seam decrease, following a generally linear downward trend in the curves.

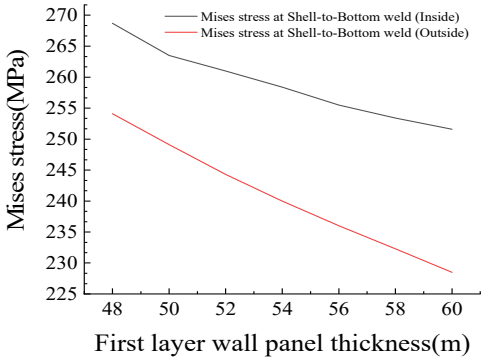

Fig. 6. Maximum stress versus wall thickness curve at the shell-to-bottom weld.

4 Study on the Influence of Bottom Plate Size on Stress

4.1 The Influence of Edge Plate Extension Length

Under the combined action of lateral pressure from the molten salt, friction from the bottom plate, and high-temperature expansion, the shell-to-bottom weld area often

tends to rotate. The extended part of the edge plate can serve as a constraint on this rotation. Therefore, it is necessary to study the influence of the edge plate's extension length on the stress distribution in the shell-to-bottom weld area. In this study, the extension lengths of the edge plate were selected as 0 mm, 50 mm, 100 mm, 150 mm, 200 mm, 250 mm, and 300 mm.

Fig. 7 illustrates the stress variation on the lower side of the bottom plate for different edge extension lengths. When the extension length is 0mm, stress paths on the bottom plate exhibit two extreme points: the first extreme corresponds to the inner side of the tank wall at the bottom plate position from left to right, and the second extreme corresponds to the outermost edge of the bottom plate. As the extension length increases, the stress at these two points gradually decreases.

For non-zero extension lengths, a third stress extreme appears between the first and second points, corresponding to the outer side of the tank wall at the bottom plate position. As the extension length increases further, the Mises stress at this point continues to rise until reaching a constant value at 200mm extension length.

In summary, at an extension length of 150mm, the stresses at the three extreme points mentioned above are relatively balanced. For other extension lengths, there may be cases where the stress at one extreme point is significantly higher. Therefore, selecting an extension length of 150mm for the edge plate is deemed reasonable based on the stress curves discussed earlier.

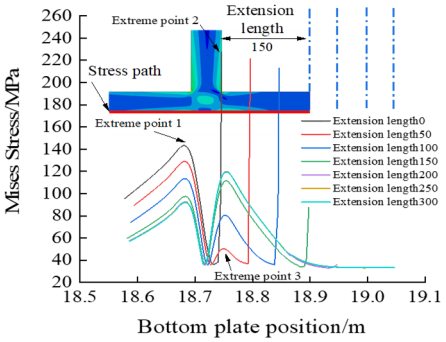

Fig. 7. Bottom plate stress path curves for different edge plate extension length

Fig. 8 shows the variation curves of the maximum Mises stress on the inner and outer sides of the shell-to-bottom weld with different edge plate extension length. For the inner side, the stress curve increases as the extension length changes from 0mm to 50mm, then decreases as the extension length continues to increase. The outer side shows the opposite trend, with the stress curve decreasing from 0mm to 50mm and then increasing as the extension length increases further.

At an extension length of 150mm, the Mises stress on both the inner and outer sides is approximately equal, indicating a more uniform stress distribution in the shell-to-bottom weld region. When the extension length exceeds 200mm, the extension length has little to no effect on the stress on both the inner and outer sides of the shell-to-bottom weld.

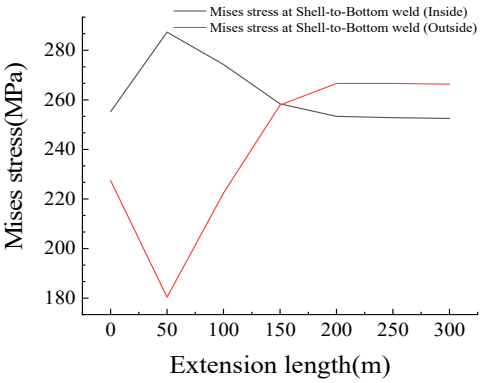

Fig. 8. Maximum stress variation curve of the shell-to-bottom weld with different extension lengths

Fig. 9 shows the stress variation curves on the inner and outer sides of the first layer of the tank wall with different edge plate extension lengths. The figure indicates that changes in the extension length affect the first layer wall panel within the height range of 0m to 1.5m, with minimal impact on the stress of the wall panel between 1.5m and 2.5m. Additionally, as the extension length increases, the point of minimum stress on the curve gradually shifts to the left, indicating that the height of the minimum stress point on the first layer wall panel decreases.

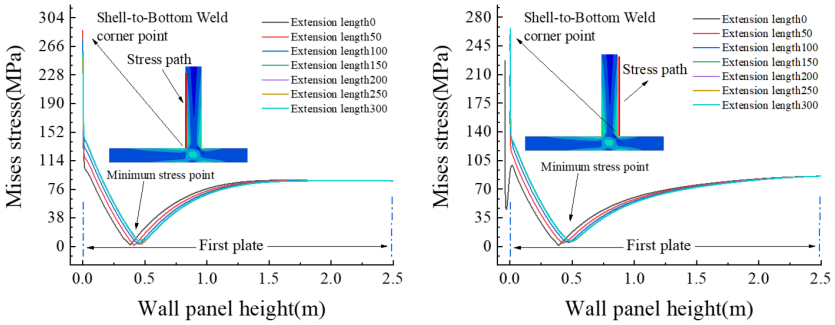

Fig. 9. Stress variation curves of the first layer of the tank wall with different edge plate extension lengths: (a) Inner side (b) Outer side

Fig. 10(a) shows the deformation distribution of the bottom plate with different edge plate extension lengths. The figure indicates that when the edge plate extension length changes, the bottom plate near the shell-to-bottom weld deforms upwards, resulting in detachment from the foundation. With smaller extension lengths, the height of the bottom plate detachment from the foundation is greater, and the width of the detached portion is also larger.

Fig. 10(b) shows the relationship between the maximum height of bottom plate detachment from the foundation and the edge plate extension length. As the extension length increases, the detachment height gradually decreases. When the extension length reaches 200mm, further increasing the extension length does not reduce the detachment height.

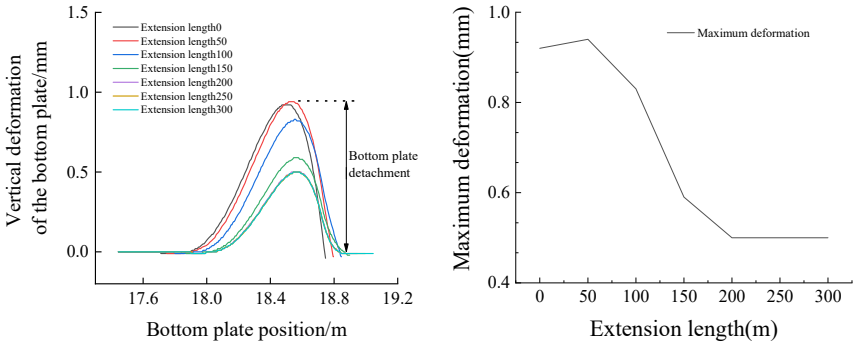

Fig. 10. (a) Vertical deformation distribution curves of the bottom plate with different edge plate extension lengths. (b) Relationship curve between the maximum detachment height of the bottom plate and the edge plate extension length.

4.2 The Influence of Bottom Plate Thickness

The welding between the first edge plate and the first layer of the wall plate forms the shell-to-bottom weld area. This area not only bears the self-weight pressure of the upper wall plate but also generates significant friction with the foundation due to thermal expansion. Therefore, it is essential to study the effect of edge plate thickness on the stress distribution in the shell-to-bottom weld area. In this study, the thicknesses of the first ring of the annular edge plate were selected as 37 mm, 39 mm, 41 mm, 43 mm, 45 mm, 47 mm, and 49 mm, respectively.

Fig. 11 illustrates the stress path curves of the bottom plate at different bottom plate thicknesses. The horizontal axis represents the distance extending from the inner to the outer side of the first ring of annular edge plate. There are three stress extremum points on the stress path curve: the first stress extremum point is located in the middle of the first ring of annular edge plate, and the second and third stress extremum points are located at the positions of the wall plate. From the graph, it is evident that the stress extremum points of the bottom plate decrease with increasing bottom plate thickness.

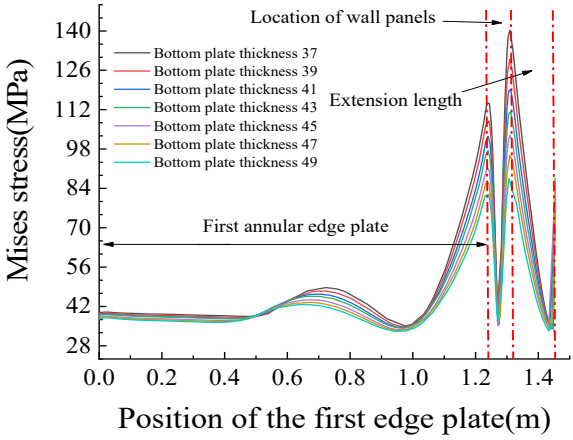

Fig. 11. Stress path curves of the bottom plate at different bottom plate thicknesses

Fig. 12 depicts the relationship between the maximum Mises stress on the inner and outer sides of the shell-to-bottom weld and the thickness of the first ring of annular edge plate. The graph shows that with increasing thickness of the first ring of annular edge plate, the maximum stress on the outer side of the shell-to-bottom weld decreases linearly. However, the variation in bottom plate thickness does not affect the maximum stress on the inner side of the shell-to-bottom weld, which remains around 257 MPa.

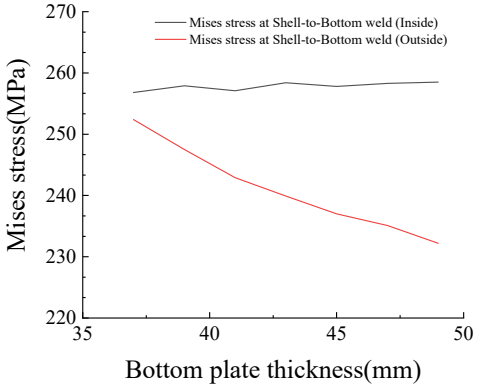

Fig. 12. Relationship curves between the maximum Mises stress on the inner and outer sides of the shell-to-bottom weld and the thickness of the first ring of annular edge plate.

Fig. 13 shows the vertical deformation distribution curves of the bottom plate and the variation of the maximum detachment height with different thicknesses of the first ring of annular edge plate. The graph illustrates that increasing the bottom plate thickness causes the maximum detachment height to decrease continuously, following a linear trend. Additionally, the change in bottom plate thickness does not affect the width range of the bottom plate detachment from the foundation.

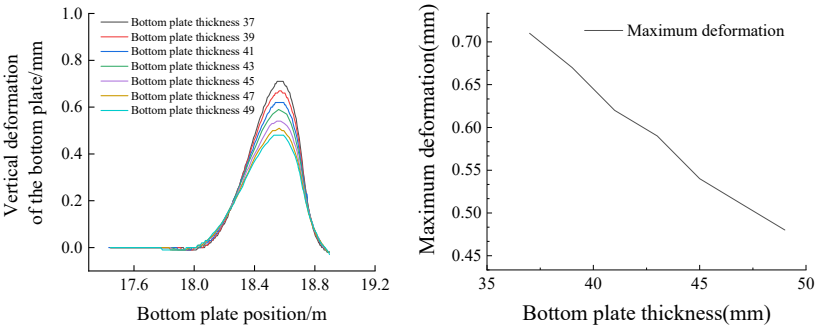

Fig. 13. (a) Vertical deformation distribution curves of the bottom plate with different thicknesses of the first ring of annular edge plate. (b) Relationship curve between the maximum detachment height of the bottom plate and the thickness of the first ring of annular edge plate.

5 Conclusion

Through extensive finite element numerical simulations based on a molten salt storage tank design project in Qinghai Province, this study conducted a parametric investigation on various geometric dimensions at the location of the shell-to-bottom weld. It examined the effects of the first layer wall plate thickness, edge plate extension length, and edge plate thickness on the tank's stress and deformation. The conclusions drawn from the study are summarized as follows:

1. Increasing the thickness of the first layer wall plate primarily affects the stress of the first layer wall plate, significantly reducing the Mises stress at a height of 1.5m and having a smaller impact at 2.5m. The peak stress at the shell-to-bottom weld decreases significantly with an increase in wall plate thickness.

2. The edge plate extension length has a significant impact on the stress of the bottom plate. When the extension length is too small or too large, there are significant stress extremum points on the bottom plate, and there is a large difference in stress between the inner and outer sides of the shell-to-bottom weld. When the extension length is 150mm, the stress extremum points on the bottom plate are more evenly distributed, and the difference in maximum stress between the inner and outer sides of the shell-to-bottom weld is smaller. The edge plate extension length should not be too small or too large, and should be determined based on the results of finite element analysis.

3. A larger edge plate extension length results in a narrower range of detachment width of the bottom plate from the foundation and a smaller maximum detachment height. When the extension length exceeds 200mm, it has no significant effect on the stress of the bottom plate, shell-to-bottom weld stress, and bottom plate deformation.

4. Increasing the thickness of the first ring edge plate significantly reduces the stress of the bottom plate and the maximum stress on the outer side of the shell-to-bottom weld, while it has no effect on the maximum stress on the inner side of the shell-to-bottom weld. Increasing the bottom plate thickness reduces the maximum detachment

height from the foundation but does not affect the width range of detachment from the foundation.

5. Compared to the bottom plate thickness, the wall plate thickness has a greater impact on the maximum stress in the shell-to-bottom weld region. Therefore, in the design process, if it is necessary to control the maximum stress in the shell-to-bottom weld, increasing the wall plate thickness should be considered first. And the selection of thickness should be balanced with engineering costs.

In summary, this study provides valuable references for the subsequent engineering design of molten salt storage tanks through extensive finite element parameter calculations. However, there are still some issues that require further research and discussion due to the complexity of the problem and the simplifications made in the finite element model.

1. This study only investigated the three main geometric dimensions of the shell-to-bottom weld area. Further research is needed to examine the influence of other parameters on the stress distribution in the shell-to-bottom weld area.

2. Integration with the calculation methods specified in the API 650 standard is necessary to optimize the geometric dimensions of the shell-to-bottom weld area.

References

1. BURGALETA J, ARIAS S, RAMIREZ D. Gemasolar, the first tower thermosolar commercial plant with molten salt storage [J]. Solarpaces, 2011, 69.
2. ZAVERSKY F, GARCíA-BARBERENA J, SáNCHEZ M, ASTRAIN D. Transient molten salt two-tank thermal storage modeling for CSP performance simulations [J]. Solar Energy, 2013, 93: 294-311.
3. PRICE H, MEHOS M, KEARNEY D, et al. Chapter 20 - Concentrating solar power best practices [M]//LOVEGROVE K, STEIN W. Concentrating Solar Power Technology (Second Edition). Woodhead Publishing. 2021: 725-57.
4. ZENG X, WANG X, LI H, QIAN C. Strength and Creep-Fatigue Analysis of a Molten-Salt Storage Tank; proceedings of the 2019 International Conference on Artificial Intelligence and Advanced Manufacturing (AIAM), F 16-18 Oct. 2019, 2019 [C].
5. TANG Z, TAO W-Q. Strength analysis of molten salt tanks for concentrating solar power plants [J]. Energy Storage and Saving, 2023, 2(4): 571-7.
6. ZHANG X, WU Y, ZHANG C. Temperature Distribution and Strength Analysis of Large-scale Molten Salt Thermal Storage Tank [J]. Journal of Beijing University of Technology, 2021, 47(9): 1064-73.
7. XIAOXIAO G. Structure Design and Performance Study of Molten Salt Tank [D], 2018.
8. WAN Z, WEI J, QAISRANI M A, et al. Evaluation on thermal and mechanical performance of the hot tank in the two-tank molten salt heat storage system [J]. Applied Thermal Engineering, 2020, 167: 114775.
9. XIAOMING Z, YUTING W, CANCAN Z. Temperature Distribution and Strength Analysis of Large-scale Molten Salt Thermal Storage Tank [J]. JOU R NAL OF BEIJING UNIVE R SITY OF TECHNOLOGY, 2021, 47(09): 1064-73.
10. API Welded Steel Tanks for Oil Storage, 12th Edition, Includes Errata (2013) and Addenda 1 (2014) and 2 (2016) / Tank Inspection, Repair, Alteration, and Reconstruction, 5th Edition Set: [S]. 2014: